

# The AMIGA sample of isolated galaxies

## VI. Radio continuum properties of isolated galaxies: a very radio quiet sample

S. Leon<sup>1,2</sup>, L. Verdes-Montenegro<sup>2</sup>, J. Sabater<sup>2</sup>, D. Espada<sup>3</sup>, U. Lisenfeld<sup>4</sup>, A. Ballu<sup>5</sup>, J. Sulentic<sup>6</sup>, S. Verley<sup>7</sup>,  
 G. Bergond<sup>2</sup>, and E. García<sup>2</sup>

<sup>1</sup> Instituto de Radioastronomía Milimétrica (IRAM), Avenida Divina Pastora 7, Núcleo Central, 18012 Granada, Spain  
 e-mail: leon@iram.es

<sup>2</sup> Instituto de Astrofísica de Andalucía, CSIC, Apdo. 3004, 18080 Granada, Spain

<sup>3</sup> Institute of Astronomy and Astrophysics, Academia Sinica, No.1, Roosevelt Rd, Sec. 4, Taipei 10617, Taiwan

<sup>4</sup> Departamento de Física Teórica y del Cosmos, Facultad de Ciencias, Universidad de Granada, Spain

<sup>5</sup> École Nationale Supérieure de Physique, Université Louis Pasteur, Strasbourg, France

<sup>6</sup> Department of Astronomy, University of Alabama, Tuscaloosa, USA

<sup>7</sup> INAF-Osservatorio Astrofisico di Arcetri, Largo E. Fermi 5, 50125 Firenze, Italy

Received XX; accepted XX

### ABSTRACT

**Context.** This paper is part of a series describing the results of the AMIGA (Analysis of the interstellar Medium of Isolated GALaxies) project, studying the largest sample of very isolated galaxies in the local Universe.

**Aims.** The study of the radio properties of the AMIGA sample is intended to characterize the radio continuum emission for a sample least affected by local environment, thus providing a reference against which less isolated and interacting samples can be compared.

**Methods.** Radio continuum data at 325, 1420 and 4850 MHz were extracted from the WENSS, NVSS/FIRST and GB6 surveys, respectively. The source extractions have been obtained from reprocessing the data and new detections have been added to the cross-matched detections with the respective survey catalogs. We focus on the complete AMIGA subsample composed of 719 galaxies.

**Results.** From the above four surveys a catalog of radio fluxes was obtained. Comparison between the NVSS and FIRST detections indicates that the radio continuum is coming from disk-dominated emission in spiral galaxies, in contrast to the results found in high-density environments where nuclear activity is more frequent. The comparison of the radio continuum power with a comparable sample, which is however not selected with respect to its environment, the Condon et al. UGC-SF sample of star-forming field galaxies, shows a lower mean value for the AMIGA sample. We have obtained radio-to-optical flux ratios ( $R$ ) using the NVSS radio continuum flux. The distribution of  $R$  for the AMIGA galaxies is consistent with a sample dominated by radio emission from star formation (SF) and a small number of Active Galactic Nuclei (AGN), with less than 3% of the sample with  $R > 100$ . We derived the radio luminosity function (RLF) and total power density of the radio continuum emission for the AMIGA sample at 1.4 GHz, and compared them with results from other low redshift studies. The Schechter fit of the RLF indicates a major weight of the low-luminosity galaxies.

**Conclusions.** The results indicate the very low level of radio continuum emission in our sample of isolated galaxies, which is dominated by mild disk SF. It confirms hence the AMIGA sample as a suitable template to effectively quantify the role of interactions in samples extracted from denser environments.

**Key words.** galaxies : evolution – galaxies: luminosity function – radio continuum: galaxies – surveys

## 1. Introduction

Although it is widely accepted that galaxy interactions stimulate secular evolutionary effects in galaxies (e.g. excess star formation, active nuclei, morphological/kinematic anomalies) the frequency/amplitude of the effects and processes driving them are not well quantified. Prior to about 1970 there was a general belief that interactions did not stimulate unusual activity in galaxies. Radio continuum surveys of galaxy pairs emission statistics opened a debate about the role of interactions in stimulating activity (Tovmassian 1968). The period around 1970 saw several studies reporting a lack of radio continuum enhancement in interacting galaxies (Allen et al. 1973; Wright 1974) closely followed by several surveys that provided evidence for an enhanced level of emission from pairs (Sulentic 1976a, 1976b; Stocke 1978; Stocke et al. 1978). As the fulcrum shifted in favor of interaction induced activity, the debate shifted to the relative response of disk versus nucleus as the source of enhanced emis-

sion (Hummel 1980, 1981). Eventually evidence emerged for excess emission from both nuclei and disks (Condon et al. 1982). Not surprisingly spiral galaxies have provided the strongest evidence for a radio enhancement, but recently, evidence has also arisen for radio continuum enhancements in early-type members of mixed pairs (E/S0+S), possibly via cross-fueling from a gas rich neighbor (Domingue et al. 2005). Interactions apparently do not always lead to enhancement, as evidenced by compact groups where radio emission is weaker than average, although more strongly concentrated than in more normal galaxies (Menon 1992, 1995, 1999).

A better quantification of interaction enhancement as a function of many different observables is needed before models can be properly constrained and refined. This requires a proper definition of non-interacting galaxy in order to determine the “zero-point” or levels of self stimulated emission (nature vs. nurture). The AMIGA project (Analysis of the interstellar Medium of

Isolated GALaxies) involves identification and parameterization of a statistically significant sample of the most isolated galaxies in the local Universe. It is a refinement of the Catalog of Isolated Galaxies (CIG; Karachentseva 1973) which is composed of 1050 galaxies located in the Northern hemisphere. A major AMIGA goal involves characterization of different phases of the interstellar medium in galaxies least affected by their environment.

So far we have: 1) revised all CIG positions (Leon & Verdes-Montenegro 2003); 2) summarized the redshift and luminosity properties of the sample including derivation of an improved Optical Luminosity Function (Verdes-Montenegro et al. 2005); 3) provided POSS2 based morphologies for the sample including identification of remaining certain (32) and suspected (161) interacting galaxies (Sulentic et al. 2006); 4) reevaluated the IRAS mid-infrared and far-infrared properties of the sample (Lisenfeld et al. 2007); and 5) performed a reevaluation and quantification of the degree of isolation for the sample (Verley et al. 2007a, 2007b). The revised CIG-AMIGA sample is reasonably complete ( $\sim 80\%$ ) down to  $m_{B-\text{corr}} \sim 15.0$  (Verdes-Montenegro et al. 2005) and is currently the largest sample of isolated galaxies in the local Universe. These are galaxies whose structure and evolution have been driven largely or entirely by internal rather than external forces (i.e. as close to pure nature as exists in a local Universe where nurture plays many roles). The data are being released and periodically updated at <http://www.iaa.es/AMIGA.html> where a VO (Virtual Observatory) interface with different query modes has been implemented.

We report here on the radio continuum properties of the AMIGA sample with presentation organized as follows: Section 2 describes the radio surveys we used along with the (reprocessed) data and the final catalogs. Section 3 studies the radio continuum characteristics of the AMIGA sample including the correlation between radio and optical luminosities, spectral index, as well as comparison between NVSS and FIRST measures. The Radio Luminosity Function (RLF) and the power density are presented and compared with other galaxy samples in Sect. 4. Section 5 summarizes the main results.

## 2. The radio data

Several radio surveys now cover a large fraction of the sky with detection limits of a few mJy and spatial resolutions from a few arcseconds to a few arcminutes. Four Northern sky surveys are available: 1) the Westerbork Northern Sky Survey (WENSS) at 325 MHz; 2) the NRAO VLA Sky Survey (NVSS) at 1.4 GHz; 3) the Faint Images of the Radio Sky at Twenty-cm survey (FIRST) at 1.4 GHz; and 4) the Green Bank surveys (GB6) at 4.8 GHz. We cross-correlated the optically improved AMIGA positions (Leon & Verdes-Montenegro 2003) with radio source positions from the above catalogs and further increased detection fractions by reprocessing source extractions from the calibrated data. Extractions were performed using the dedicated software SExtractor (Bertin & Arnouts 1996) with a threshold of  $5\text{-}\sigma$  relative to the background. A summary of the data extracted from the four surveys is given in Table 1. The  $N_{\text{CIG}}$  and  $N_{\text{det}}$  entries indicate respectively the number of galaxies that were covered by each survey and the number of detections. Table 2 gives the radio flux density, the radio power, and a code for the origin of the data according to the following list: 0 for no data, 1 for the original catalog (WENSS, NVSS, GB6), 2 for this work and 3 for NED. Reference code 4 indicates FIRST detection without a corresponding NVSS detection. Upper limits are indicated by negative values. 1420 MHz FIRST measures follow in parentheses

**Table 1.** Compiled data for the different radio continuum surveys.

Survey	Frequency (MHz)	Resol. (arcmin)	$5\text{-}\sigma$ (mJy)	$N_{\text{CIG}}^1$	$N_{\text{det}}^1$
WENSS	325 & 352	$\sim 1$	$\sim 18$	405/278	49/37
NVSS	1420	$\sim 0.8$	$\sim 2$	1050/719	374/311
FIRST	1420	$\sim 0.08$	$\sim 1$	560/360	81/58
GB6	4850	$\sim 3.5$	$\sim 18$	1017/691	32/12

<sup>1</sup> Total number of galaxies with radio data ( $N_{\text{CIG}}$ ) and with radio detection ( $N_{\text{det}}$ ), followed by the number of galaxies belonging to the complete subsample of  $N = 719$  galaxies.

the NVSS values. Fluxes of the 8 galaxies detected with FIRST and undetected with the NVSS are listed in Table 2 but are not used in the analysis as explained in Sect. 2.3. Radio power  $P$  was computed as  $\log(P) = \log(\frac{S}{\text{mJy}}) + 2 \log(\frac{D}{\text{Mpc}}) + 17.08$ . We used distances  $D$  from Verdes-Montenegro et al. (2005) with a Hubble constant of  $H_0 = 75 \text{ km s}^{-1} \text{ Mpc}^{-1}$  updated with the newly available data from the bibliography. The small number of sources without radio power values lack redshifts. The next subsections describe the four surveys used to characterize the radio continuum properties of our sample.

We derived radio fluxes or upper limits for all galaxies in the CIG but we focus our statistical analysis on the complete AMIGA subsample described in Verdes-Montenegro et al. (2005). We use in the present work the same selection as described in Lisenfeld et al. (2007) (their Sect. 4.1): (i) The subsample contains galaxies with corrected Zwicky magnitudes in the range 11.0–15.0 for which we found  $\langle V/V_m \rangle = 0.43$ , indicating 80–90% completeness. (ii) Morphological revision of the sample, described in Sulentic et al. (2006), identified 32 galaxies that are probably not isolated in the sense that they might involve isolated interacting pairs and/or multiplets. These galaxies are excluded from the most isolated sample studied further here. (iii) We excluded two nearby dwarf ellipticals (CIG 663  $\equiv$  Ursa Minor and CIG 802  $\equiv$  Draco) for which we only have upper limits for the radio fluxes, and the inferred radio luminosities are very low. This subsample ( $N = 719$  galaxies) will be referred to hereafter as the complete (AMIGA) subsample.

### 2.1. WENSS

The WENSS (Rengelink et al. 1997) survey was carried out with the Westerbork Synthesis Radio Telescope at 325 MHz, except for objects with  $\delta > 30^\circ$  that were observed at 352 MHz. Spatial resolution is  $\theta_{\text{WENSS}} \approx 54'' \times 54'' \text{ cosec}(\delta)$  with limiting flux sensitivity of about 18 mJy ( $5\text{-}\sigma$ ). Astrometric accuracy was  $1''.5$  for strong sources ( $S > 150 \text{ mJy}$ ). We adopted a distance tolerance of  $35''$  which was chosen taking into account a conservative astrometry accuracy for weak sources of  $\approx \theta_{\text{WENSS}}/5$  and adopting a confidence radius  $\sim 3$  times that value. We found 39 WENSS detections. Five more detections were included from the 352 MHz polar catalog (CIG 66, 155, 363, 875 and 890).

We also downloaded and reprocessed source extractions for other galaxies from the CIG that are within in the survey area. Flux calibrations using the integrated SExtractor fluxes of catalog sources show no significant differences from the WENSS catalog values. A total of 49 sources were detected and 404 upper limits derived. Five weak sources were not listed in the WENSS catalog (CIG 336, 355, 663, 676 and 862) but are de-

tected at a  $5\text{-}\sigma$  level using SExtractor, showing a very weak emission ( $< 18$  mJy). The total flux for the extended source CIG 442 was underestimated and recomputed taking extended emission into account. The astrometry accuracy is very high, the mean difference with respect to the CIG position being  $(\alpha, \delta) = (0''.08, 0''.34)$ . The dispersion in the  $\alpha$  and  $\delta$  differences are respectively  $6''.4$  and  $9''.3$  which is about 6–9 times smaller than the WENSS spatial resolution.

## 2.2. NVSS

The NVSS survey (Condon et al. 1998) was made with the VLA at 1.4 GHz. Spatial resolution was  $45'' \times 45''$  for North of  $\delta > -40^\circ$ , covering the full CIG declination range. Survey sensitivity is about 2 mJy implying that nearly all sources detected with WENSS (assuming spectral index  $\alpha_{0.3}^{1.4} > -1.5$ ) will be detected by NVSS. Source positions in the catalog are given with an accuracy ranging from  $< 1''$  for flux density  $S > 15$  mJy to about  $7''$  for  $S < 2.5$  mJy. We found 359 CIG sources in the NVSS catalog. Source extraction using SExtractor with a  $5\text{-}\sigma$  threshold yielded 368 detections, where 9 are not in the NVSS catalog or were recalibrated in cases of extended or weak sources (CIG 324, 436, 442, 543, 559, 837, 869, 950, 988). CIG 199 was excluded from the catalog because of corrupted data.

Comparison of fluxes derived from the NVSS catalog and our reprocessing (see Fig. 1) indicates a high degree of concordance except for an increasing dispersion and underestimation towards fainter fluxes. These small differences are probably due to the bias corrections applied to fluxes in the NVSS catalog and which were not fully taken into account in the reprocessed fluxes. This difference in calibration affects only the few sources not listed in the NVSS catalog. In the case of very extended sources ( $> 5''.5$ ; CIG 197, 435, 447, 461, 469, 610) we have adopted fluxes given in the literature (NED). In these cases, the total flux was computed from a complete integration over the galaxy and not only from some isolated peaks, as given by the NVSS for the large and nearby galaxies. A final total of 374 galaxies are included with 1.4 GHz radio continuum detections. The mean difference in  $\alpha$  and  $\delta$  between the NVSS and our catalog positions are small ( $-0''.83, -0''.02$ ). The dispersion in the  $\alpha$  and  $\delta$  differences are respectively  $6''.9$  and  $7''.2$ , which is comparable to the WENSS astrometry given the similar spatial resolution.

## 2.3. FIRST

FIRST (Becker et al. 1995) was designed to produce the radio equivalent of the Palomar Observatory Sky Survey over 10 000 square degrees of the North Galactic Cap. The spatial resolution was  $5''$ . At the 1 mJy source detection threshold there are  $\sim 90$  sources per square degree,  $\sim 35\%$  of which show resolved structure on scales from  $2''$  to  $30''$ . We cross-correlated the FIRST catalog with our revised optical positions, yielding 81 source detections. The number of detections was low and the data could not be used for statistical purposes. They were however very useful for a comparison with NVSS data which allowed us to infer the relative strengths of disk vs. nuclear emission in many galaxies. Mean positional differences are small ( $-0''.22, -0''.07$ ) with a dispersion of  $1''.6$  and  $2''.0$ , respectively. We found 8 galaxies that were detected in FIRST but not in the NVSS (CIG 236, 238, 258, 364, 544, 618, 678 and 749). Normally we expect the NVSS flux to be stronger than the FIRST values because FIRST is only sensitive to compact (high spatial frequency) radio emission. These

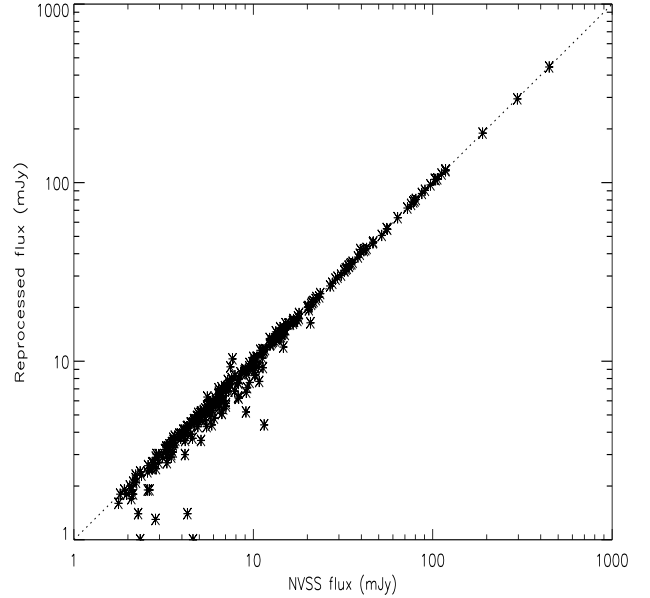


**Fig. 1.** Comparison of the NVSS catalog flux (abscissa) at 1.4 GHz and the reprocessed fluxes for the CIG sources (ordinates).

sources showed fluxes near the NVSS/FIRST detection limits and were not further considered in our analysis.

## 2.4. GB6

The GB6 survey is a combination of two sets of observations made at the Green Bank telescope in 1986 and 1987 (Gregory et al. 1996). The sensitivity of the survey is similar to WENSS ( $\sim 18$  mJy) but the spatial resolution is considerably lower ( $3''.5$ ). Identification of CIG detections in the GB6 catalog required a threshold distance tolerance of about  $1/2$  of the FWHM, i.e.  $85''$  which results in 17 detections. SExtractor source extraction with a detection threshold of  $5\text{-}\sigma$  yields 42 detections within the  $85''$  confidence radius. Comparison of our fluxes with GB6 catalog values indicates a poorer correlation. Discrepancies mainly arise from extended sources. The large spatial resolution compared with the galaxy diameters motivated a visual check of all detections in order to remove possible cases of confusion. A total of 32 galaxies were retained in our GB6 detection list, with others determined to be fore-/back-ground.

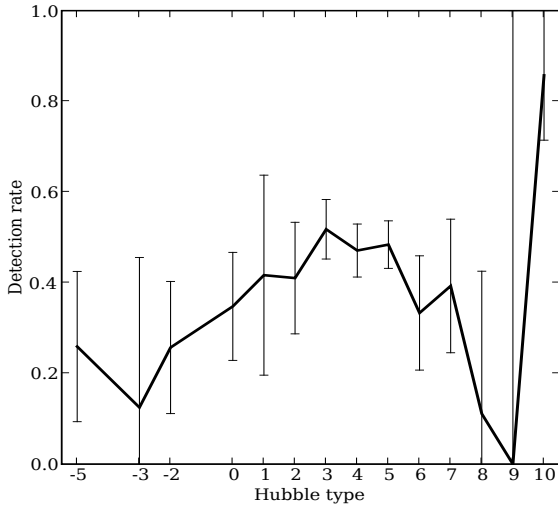
## 3. Radio characteristics

### 3.1. Detection rate

Figure 2 shows the NVSS radio detection fraction as a function of morphological type (see Sulentic et al. 2006 for a description of the morphological types). It peaks in the Sb–Sc range (type  $T = 3\text{--}5$ ) which is the core of the AMIGA sample, comprising fully two thirds of our sample (see Verdes-Montenegro et al. 2005). Assuming that the radio continuum emission is driven by star formation this is not surprising because these galaxies show the highest average star formation rates (Kennicutt et al. 1987). This is partially offset by the higher molecular/neutral gas fraction found in earlier types (Young & Knezek 1989) which may explain why the detection fraction drops so slowly towards types earlier than  $T = 3$  (Sb). This can be contrasted to the much more rapid drop in the FIR detection fraction found in Lisenfeld et al.

**Table 2.** Radio flux density and power 325 MHz, 1.4 GHz and 4.8 GHz for the CIG sample<sup>1</sup>.

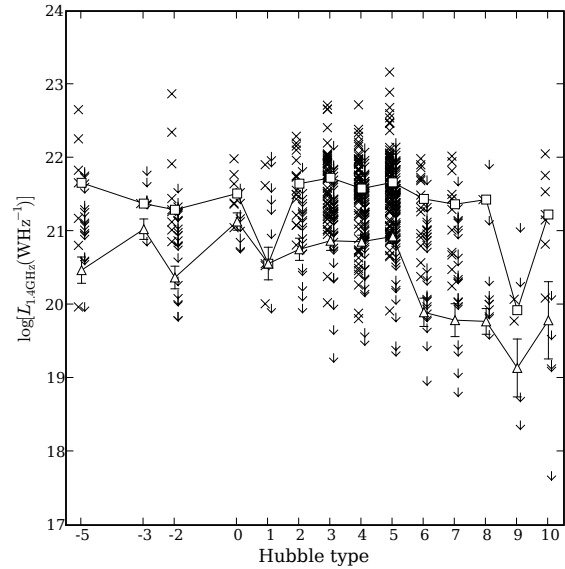
CIG	325 MHz			Ref.	1.4 GHz			Ref.	4.8 GHz			Ref.
	Flux (mJy)	Error (mJy)	Power (W Hz <sup>-1</sup> )		Flux (mJy)	Error (mJy)	Power (W Hz <sup>-1</sup> )		Flux (mJy)	Error (mJy)	Power (W Hz <sup>-1</sup> )	
1	0.00	0.00	0.000	0	7.70	0.72	21.894	1	-18.00	0.00	-22.262	1
2	-18.00	0.00	-22.228	1	-2.00	0.00	-21.274	1	-18.00	0.00	-22.228	1
3	-18.00	0.00	0.000	1	-2.00	0.00	0.000	1	-18.00	0.00	0.000	1
4	0.00	0.00	0.000	0	31.70	1.07	21.412	1	-18.00	0.00	-21.166	1
5	0.00	0.00	0.000	0	-2.00	0.00	-21.380	1	-18.00	0.00	-22.335	1
6	0.00	0.00	0.000	0	6.10	0.66	21.356	1	-18.00	0.00	-21.826	1
7	0.00	0.00	0.000	0	-2.00	0.00	-21.815	1	-18.00	0.00	-22.769	1
8	0.00	0.00	0.000	0	-2.00	0.00	-21.183	1	-18.00	0.00	-22.137	1
9	0.00	0.00	0.000	0	2.40	0.79	21.526	1	-18.00	0.00	-22.402	1
10	-18.00	0.00	-21.852	1	-2.00	0.00	-20.897	1	-18.00	0.00	-21.852	1
...	...	...	...	...	...	...	...	...	...	...	...	...

<sup>1</sup> Full table available in electronic form at the CDS web site <http://cdsweb.u-strasbg.fr> and from <http://www.iaa.es/AMIGA.html>.**Fig. 2.** Detection rate at 1.4 GHz with NVSS as a function of Hubble type.

(2007). Alternative explanations for the relatively high detection fraction of earlier types include: 1) Sb–c spirals misclassified as Sa–ab ( $T = 1$ –2) due to low resolution imagery; 2) spirals misclassified as E/S0 ( $T = -5$  to  $-2$ ); and 3) the growing influence of radio emission unrelated to star formation in *bona fide* early types. The large fluctuation among the very late types likely involves small sample statistics.

### 3.2. Luminosity distribution

In analogy to earlier papers in this series, Fig. 3 shows the distribution of radio luminosities as a function of type for all detections. In addition, we plot mean values including upper limits which were derived using the Kaplan-Meier survival analysis and calculated with the ASURV package (Lavalley et al. 1992). Since the radio detection fraction is less than 50% for all types the mean values lie quite low relative to the detections. Note that the mean of  $\log(L)$  can be lower than the median of  $\log(L)$ . The weakest known classical radio loud quasars (FRIIs; Sulentic et al. 2003) show radio luminosities near  $\log L_{1.4\text{GHz}} = 23.5$  and the strongest sources in this sample are 0.5 dex below, with the

**Fig. 3.** Distribution of radio luminosity at 1.4 GHz as a function of Hubble type. Only detections are shown. The open triangles give the mean value of  $\log(L_{1.4\text{GHz}})$  for each Hubble type, calculated with ASURV and taking the upper limits into account. The open squares are the median values for the detections only.

majority of detected sources 1.5–2 dex below. With the exception of a few of the strongest sources all luminosities are consistent with nonthermal emission related to star formation. Figure 3 can be compared with the equivalent for FIR emission (Fig. 5 in Lisenfeld et al. 2007).

The radio power distribution for the three radio bands is shown in Fig. 4. The vertical dotted line indicates the radio power corresponding to a completeness higher than 80% (i.e., more than 80% of the galaxies are detected at the corresponding radio frequency). This line is calculated based on the sensitivity of each survey, combined with a recession velocity lower than  $9300 \text{ km s}^{-1}$  for 80% of the CIG galaxies. We point out that the peak of the distribution for the NVSS data is above the level of radio completeness, leading to a better confidence in the radio properties at that frequency. Table 3 shows the mean value of

**Table 3.** Average properties of the radio power,  $\log(P)$ , for galaxies in the complete AMIGA sample and for the 1.4 GHz radiocontinuum emission of the UGC-SF sample (Condon et al. 2002).

Frequency	Mean $\log(P)$ ( $\text{W Hz}^{-1}$ )	Median $\log(P)$ ( $\text{W Hz}^{-1}$ )	$N_{\text{gal}}$	$N_{\text{det}}$
CIG/325 MHz	$20.03 \pm 0.11$	22.24	278	37
CIG/1.4 GHz	$20.11 \pm 0.10$	21.59	719	311
CIG/4.8 GHz	$18.54 \pm 0.11$	21.53	691	12
UGC-SF/1.4 GHz	$21.61 \pm 0.62$	21.65	3136	2815

the radio power for each frequency using the Kaplan-Meier survival analysis, and the median value taking only detections into account. Note that for the 325 MHz band, the 5 galaxies with data at 352 MHz are included. The big difference between the median and mean values reflects the large number of upper limits in the samples. The number of galaxies per frequency band in the AMIGA sample is indicated in the column  $N_{\text{gal}}$ , and the number of detections by  $N_{\text{det}}$ .

We compare the radio power distribution of the CIG sample with the one of the star-forming galaxies selected from the UGC sample (UGC-SF) in Condon et al. (2002). They studied the radio and star formation properties of the entire Uppsala Galaxy Catalog (UGC). They distinguished between star-forming galaxies and AGN in their study, finding that the star-forming galaxy population may be evolving even at moderately low redshift. The AGN have been discarded of the control sample, following their classification. We recomputed the radio continuum power and the distances of the sample by using the same Hubble constant that for the CIG sample. The UGC-SF and the CIG samples are located in a very similar local volume.

To compute the mean value of the radio continuum power for the UGC-SF, we used ASURV, as for the CIG sample, by including the detections and the upper limits. The corrected  $B$  magnitude, retrieved from the LEDA database, was used for the UGC-SF sample. This photographic corrected magnitude is very similar to the  $m_{B-\text{corr}}$  magnitude of the CIG sample (see Fig. 6). To be consistent with the CIG sample, we applied a magnitude cut-off at  $m_B = 15$  (see Verdes-Montenegro et al. 2005). Using the survival analysis package ASURV, the mean of  $\log(P) = 21.61$  appears significantly higher than for the CIG sample (20.11), as shown in Table 3. The median values are computed using the detections. The difference comes mainly from the upper-limits which are a much larger fraction in the CIG sample than in the UGC-SF sample (see Table 3) with a detection rate of 43% and 90% resp. for the CIG and UGC-SF samples. Moreover the Fig. 5, showing the  $\log(P)$  distribution for both samples, indicates that the UGC-SF sample has a larger population with high radio continuum power ( $\log(P) > 22$ ).

### 3.3. Radio vs. optical properties

Since our sample involves many of the most isolated galaxies (see Verley et al. 2007a, 2007b) in the local Universe and, if radio emission is enhanced by interactions, then we expect it to show very passive radio continuum properties relative to almost any other local galaxy sample. Figure 7 compares the radio/optical flux density ratio  $R$  defined as:

$$R = S_{1.4\text{GHz}} \times 10^{0.4(m_B - 14.2)} \quad (1)$$

where  $m_B$  is the apparent  $B$  magnitude of the galaxy and  $S_{1.4\text{GHz}}$  the flux density (in Jy) at 1.4 GHz. The definition is similar to

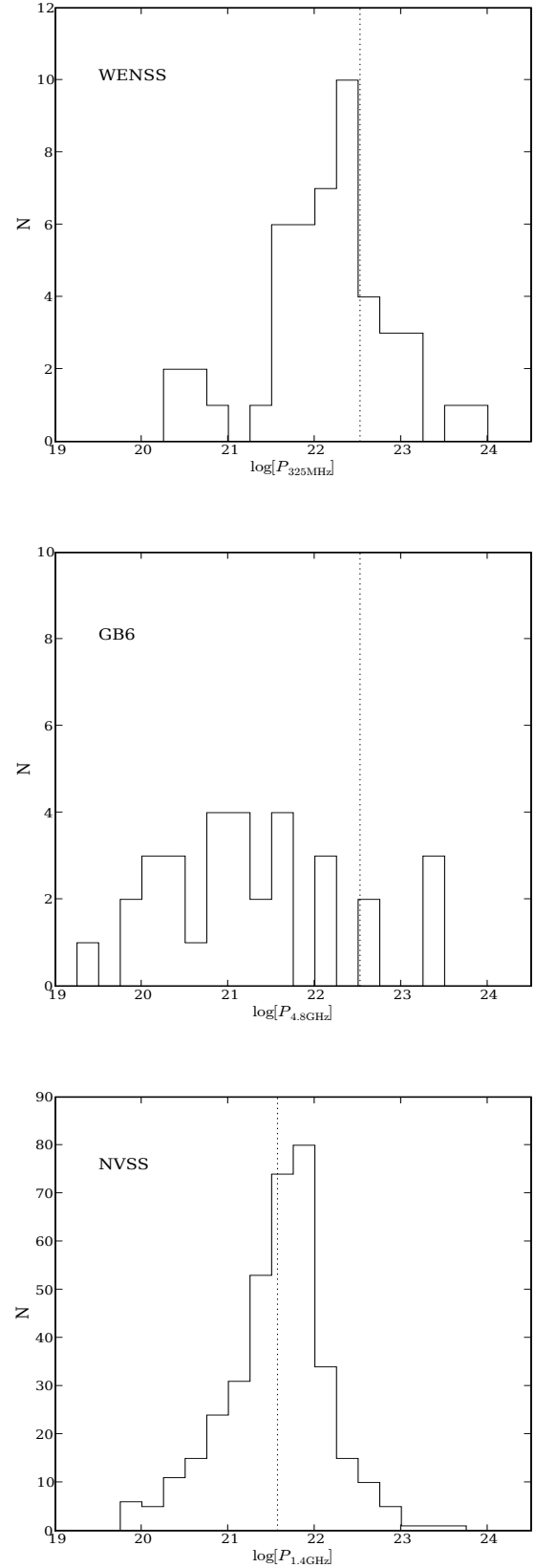


**Fig. 4.** Distribution of the 325 MHz (top), 1.4 GHz (bottom) and 4.8 GHz (middle) radio power for the CIG sample. The dotted line indicates the completeness for a velocity of  $9300 \text{ km s}^{-1}$  (80% of the sample). The  $x$ -axis indicates the logarithm of the power in  $\text{W Hz}^{-1}$ .

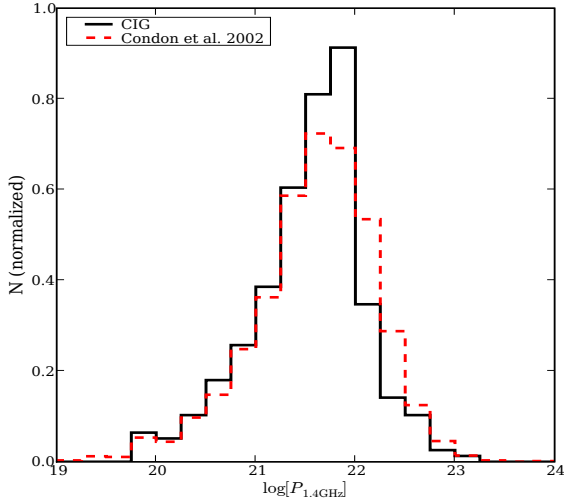


**Fig. 5.** Frequency distribution of the 1.4 GHz radio power for the CIG sample (solid line) compared with the frequency distribution of the UGC-SF sample (dashed line) of Condon et al. (2002).

the one used by Condon (1980) (the optical magnitude was normalized to 15.0 in that study).

### 3.3.1. Comparison with KISS

We chose the value  $m_B = 14.2$  for a better comparison with a sample of emission line galaxies (Van Duyne et al. 2004) which involved 207 emission-line galaxy candidates from the KPNO International Spectroscopic Survey (KISS) with NVSS or FIRST detections. Figure 8 shows the distribution of  $R$  values for detections in our sample, with E/S0 and spiral galaxies indicated separately.  $R$  shows a median value of 4.48 which is likely overestimated due to the bias introduced by the  $\sim 2$  mJy flux limit of the NVSS survey (as shown in Fig. 7 by the dashed line).

As expected, we find the galaxies in our sample to be very radio quiet relative to their optical luminosities. Generally, high values of  $R$  ( $R > 100$ , e.g. Van Duyne et al. 2004) indicate the presence of a radio quasar while values between 10 and 100 can arise from a mix of Seyfert, LINER and starburst activity. Dusty galaxies with above average internal extinction can also boost some normal galaxies into this range. The dominance of low- $R$  galaxies ( $R < 10$ ) in our sample indicates that the radio emission from star formation is responsible for the majority of the detections. The KISS sample (Van Duyne et al. 2004) represents a good counterpoint with most of the galaxies showing  $R > 10$ . Only three galaxies in our sample show  $R > 100$  (CIG 187, 349 and 836). CIG 187 has an underlying background source while CIG 349 is classified as LINER/Sy1.5 and is almost certainly an interacting/merger system. CIG 836 is a relatively high redshift E galaxy ( $V_R = 14\,900 \text{ km s}^{-1}$ ) and is outside our complete sample. 17% of the Van Duyne et al. (2004) sample show  $R > 100$ . If we consider the 11 galaxies with  $R > 30$  in our sample, we find: a) at least one background source; b) 3–5 interacting sources; and c) 4–5 AGN/LINER galaxies. Isolated examples of category c) may represent rare examples of self stimulated AGN activity (via bars?) or cases where stimulation by an accretion event left no morphological signature.

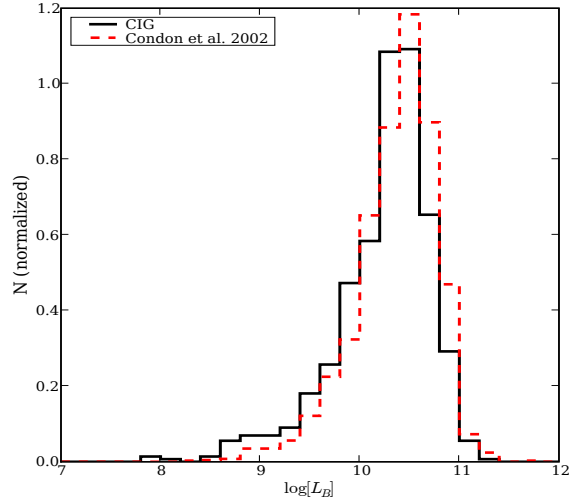


**Fig. 6.** Optical luminosity distribution in  $B$  for the CIG (solid line) and the UGC-SF (dashed line) sample.

### 3.3.2. Comparison with UGC-SF

We compare the  $R$  distribution of the CIG with the one of the UGC-SF sample of Condon et al. (2002). Figure 8 shows little differences between the two samples: the  $R$  distribution of the CIG is sharper than the one of the UGC-SF sample. This later has more important wings, especially an excess for the large  $R$  ( $\log(R) > 0.8$ ). The median value of 4.38 for  $R$  of the UGC-SF sample is just slightly larger than the one of the CIG sample (4.19). Figure 6 shows the optical luminosity  $L_B$  distribution for the CIG and the UGC-SF sample where it appears that the UGC-SF sample is slightly brighter in the  $B$  band than the CIG sample. The similar value of  $R$  between both samples is consistent with the higher radiocontinuum and  $L_B$  for the UGC-SF than for the CIG. The difference for the star formation activity is minimal between both samples, nevertheless the UGC-SF sample has a larger fraction of galaxies with more intense star formation per optical luminosity unit.

### 3.3.3. Early types

Our sample contains a relatively small fraction of early-type E/S0 galaxies ( $\sim 14\%$ ) reflecting the expectation of the morphology-density relation. In principle AMIGA provides the last point on the low density end of that correlation. The low number of early-types precludes a statistically meaningful comparison of mean  $R$  values for early- and late-type subsamples. Figure 8 suggests a slight difference between their  $R$  distributions, with median values  $R = 7.7$  and  $4.4$  for early- and late-type galaxies, respectively. The  $R$  distribution for E/S0 galaxies shows two peaks which may reflect a true early-type population and a second population of spirals misclassified as E/S0. If both peaks represent early-types then the higher  $R$  values would be surprising and difficult to understand if due to star formation activity. We checked whether either the radio powers or optical magnitudes for these galaxies had unusual values and found radio powers in the  $10^{21}$ – $10^{23} \text{ W Hz}^{-1}$  range – overlapping the radio power range of FRI but not FRII (broad emission line) quasars. Absolute magnitudes in  $B$  were generally fainter than  $-21$  (except for CIG 893 which was flagged in our morpholog-

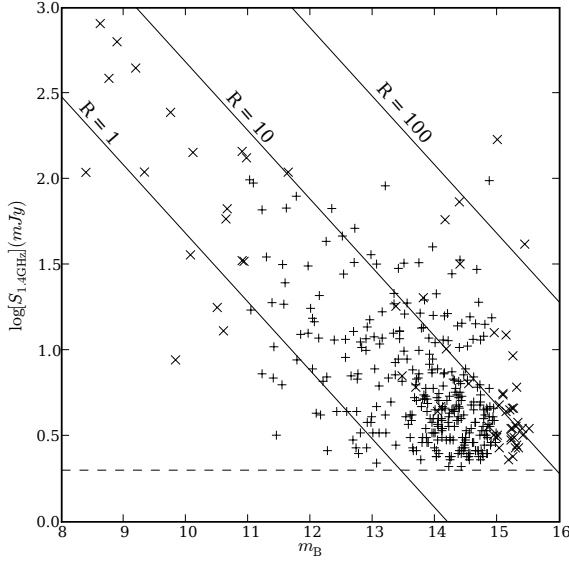


**Fig. 7.** Radio flux density at 1.4 GHz (mJy) vs. apparent  $B$  magnitude. The lines represent constant radio-to-optical ratio  $R$ . The dashed line shows the value of  $R$  corresponding to the NVSS sensitivity level (2 mJy). In order not to overload the figure, we show only detections. The radio continuum upper limits were however taken into account in the calculation of the mean values. The plus signs denote galaxies within the complete AMIGA subsample and the crosses indicate galaxies outside this subsample.

ical reclassification, in Sulentic et al. 2006, as a candidate interacting system). If confirmed as E and/or S0 galaxies, these very isolated systems would represent one of the most intriguing parts of the AMIGA sample.

### 3.4. Radio-optical luminosity correlations

The relationship between optical and radio continuum properties of galaxies in our sample can also be evaluated by studying the absolute  $B$  magnitude vs. log radio power ( $\text{W Hz}^{-1}$ ) correlation. The most useful information comes from using the 1.4 GHz data where the detection fraction was highest (Fig. 9). We use both detections and upper limits (employing survival analysis techniques) for calculation of radio continuum properties. The relation between radio continuum power and absolute  $B$  magnitude was derived using the Schmidt method (see Feigelson & Nelson 1985) as implemented in the ASURV package. A random distribution of upper limits is required for application of survival analysis techniques. In our case, the upper limit distribution of the radio power is assumed random because it was computed from a flux limited distribution combined with a random distribution of galaxy distances. We get the following relations for the complete subsample taking  $M_B$  as the independent variable:

$$\log(P_{325\text{MHz}}) = (-0.49 \pm 0.03)M_B + (11.7 \pm 0.6) \quad (2)$$

$$\log(P_{1.4\text{GHz}}) = (-0.43 \pm 0.02)M_B + (12.4 \pm 0.5) \quad (3)$$

$$\log(P_{4.8\text{GHz}}) = (-0.53 \pm 0.02)M_B + (10.6 \pm 0.5) \quad (4)$$

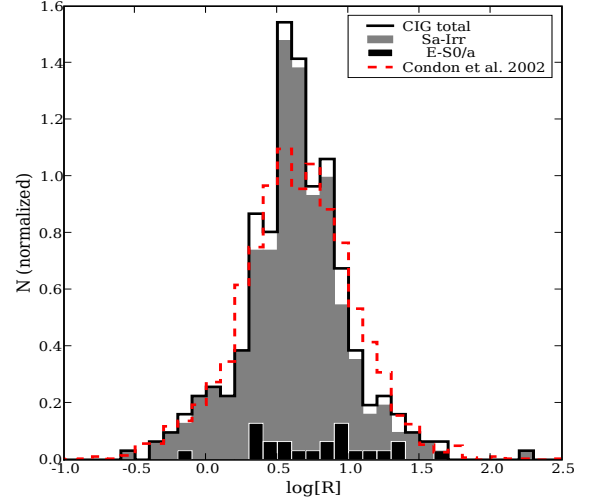


**Fig. 8.** Distribution of the radio-to-optical ratio  $R$  (logarithmic scale) for the CIG sample (solid line). The elliptical and spiral galaxy distribution are represented respectively by black and grey shaded areas. The dashed line shows the  $R$  distribution for the UGC-SF sample (Condon et al. 2002).

A bisector fit gives:

$$\log(P_{325\text{MHz}}) = (-0.60 \pm 0.03)M_B + (9.4 \pm 0.5) \quad (5)$$

$$\log(P_{1.4\text{GHz}}) = (-0.61 \pm 0.02)M_B + (8.7 \pm 0.5) \quad (6)$$

$$\log(P_{4.8\text{GHz}}) = (-0.60 \pm 0.03)M_B + (9.1 \pm 0.6) \quad (7)$$

The bisector slope of the radio power versus optical magnitude correlation is steeper at 0.3 and 4.8 GHz than at 1.4 GHz, but within the errors. In order to avoid mixing different morphological types, and hence different factors contributing to the radio emission, we derived a fit for the Sb–Sc majority population of the AMIGA sample (Fig. 9, left):

$$\log(P_{1.4\text{GHz}}) = (-0.58 \pm 0.02)M_B + (9.4 \pm 0.4) \quad (8)$$

$$(9)$$

and taking  $M_B$  as independent variable:

$$\log(P_{1.4\text{GHz}}) = (-0.39 \pm 0.02)M_B + (13.4 \pm 0.5) \quad (10)$$

$$(11)$$

Figure 9 (right) shows earlier and later type galaxies in our sample along with best fit linear regression and bisector fits to the Sb–c majority. The scatter in these relations (especially the Sb–Sc one) is still very large and will be explored in more detail in a later paper. Examination of the highest points reveals a mix of interacting systems and AGN (see Sabater et al. 2008) along with a few expected background sources. The lowest points tend to belong to highly inclined spirals, likely telling us that further refinement of inclination corrections and resultant optical luminosity corrections are needed.

It is interesting that almost all radio continuum detections of early-types lie above the best fit relation (Fig. 9, right). If the spiral majority shows radio emission related to star formation, then this offset is likely telling us that radio emission in early-types



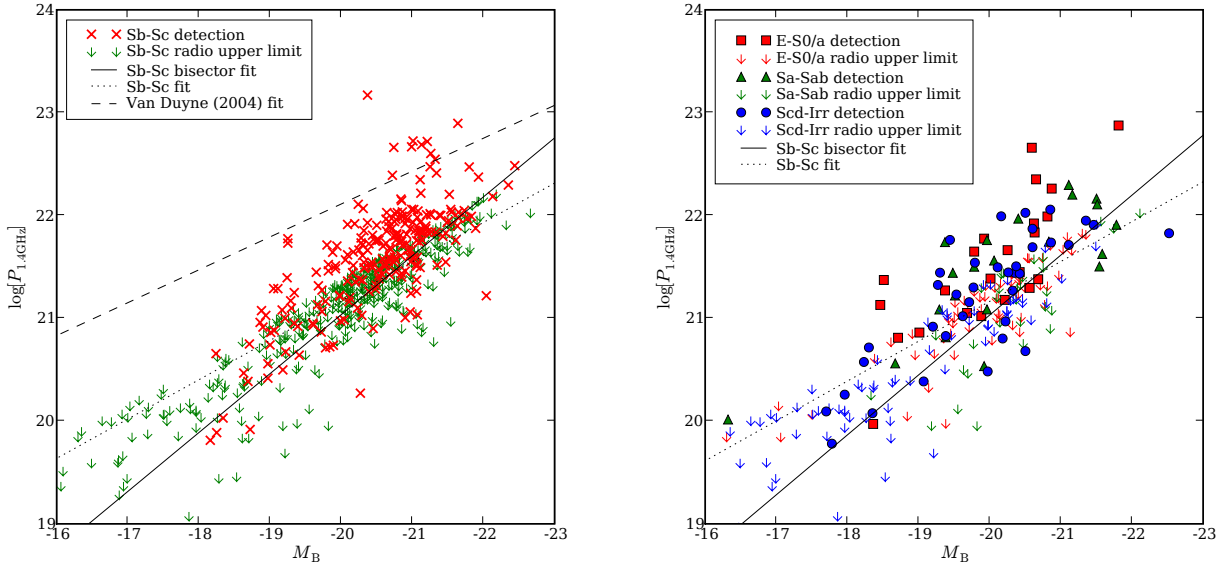


**Fig. 9. Left:** Radio power at 1.4 GHz vs. absolute optical magnitude for the Sb–Sc galaxies together with the fitted line obtained using ASURV. The full line gives the bisector fit. We also plot the fit assuming  $M_B$  as the independent variable (dotted line) for direct comparison with the fit (dashed line) for the KISS starburst galaxies in Van Duyne et al. (2004). Detections are indicated by crosses while upper limits in radio emission by arrows. **Right:** Radio power at 1.4 GHz vs. absolute optical magnitude for the detected E-S0 (filled squares), Sa-Sab (filled triangles) and Scd-Irr (filled circles) galaxies. The upper limits are indicated with arrows of the same color. The lines correspond to the same fits as in the left panel.

has a different origin. Figure 9 (left) shows that the CIG sample has a lower radio power than Van Duyne et al. (2004) over a similar absolute magnitude range. This is another manifestation of the strong difference between an emission line selected sample and our sample of isolated galaxies. Since no selection was made in the Van Duyne et al. sample in terms of the environment, it is a reasonable assumption that it involves both interacting systems and galaxies in generally higher density environments. The two samples show no sources in common.

### 3.5. Comparison between NVSS and FIRST fluxes

The NVSS and FIRST surveys were obtained with different VLA configurations, resulting in different effective resolutions and, more importantly, in diminished spatial frequency sensitivity (scales larger than  $\sim 30''$ ) for FIRST. Comparing NVSS and FIRST observations of the same source then provides insights about the spatial distribution of emission in a galaxy. FIRST will largely sample only compact (likely nuclear) emission while NVSS will detect both nuclear and disk emission from galaxies in our sample. If low level star formation dominates the radio emission from most of our galaxies, then we expect NVSS fluxes to be larger than corresponding FIRST fluxes for our sample. A strong FIRST detection might indicate an active nucleus; these sources, expected to be rare in an isolated sample like AMIGA, will be discussed in a companion paper (Sabater et al. 2008).

The much smaller FIRST detection fraction (14% vs. 35% for NVSS) immediately tells us what to expect – a sample dominated by disk star formation. FIRST fluxes are smaller than NVSS values in almost all sources. Most galaxies with a FIRST detection are Sb–Sc spirals, which represent 2/3 of the entire isolated population. This detection fraction suggests that more than half of our NVSS detected galaxies have disk-dominated

radio continuum emission at 1.4 GHz because they are fully attenuated by FIRST. Figure 10 shows the FIRST/NVSS flux ratio distribution for our sample. About 40% of the galaxies detected by FIRST show core-dominated emission at 1.4 GHz, which implies  $\sim 20\%$  of core-dominated galaxies in our sample. The radio continuum emission in core-dominated galaxies may originate either from nuclear SF or from an active nucleus. That question is addressed in Sabater et al. (2008).

We note that Menon (1995), using VLA B- and C- configurations at 1.4 GHz, found that 46/56 radio detected members of compact galaxy groups showed compact core radio emission. Figure 11 compares the cumulative distribution function of FIRST/NVSS flux ratios for AMIGA and the Menon (1995) compact group sample – a striking comparison of nature vs. nurture in the radio domain. The CDF comparison shows that only 13% of compact groups have a ratio lower than 0.5, while 36% are found for the CIGs. This shows that isolated galaxies have a more disk-dominated radio emission than galaxies in groups where extreme interaction effects are expected.

## 4. Radio Luminosity Function (RLF)

In the past few decades many researchers have studied the radio continuum properties of different samples, including derivations of the RLF. A large fraction of these studies have involved flux limited samples useful for studying the evolution of the RLF. The 1.4 GHz NRAO VLA Sky Survey (NVSS) showed that radio evolution is largely luminosity independent with strong cosmological evolution at all luminosities (Condon 1984, 1989). Benn et al. (1993) found that faint radio sources ( $S_{1.4\text{GHz}} < 1 \text{ mJy}$ ) are dominated by star-forming galaxies with only a small fraction showing Seyfert type emission. AGN dominate the bright end of the radio distribution. Galaxies from an



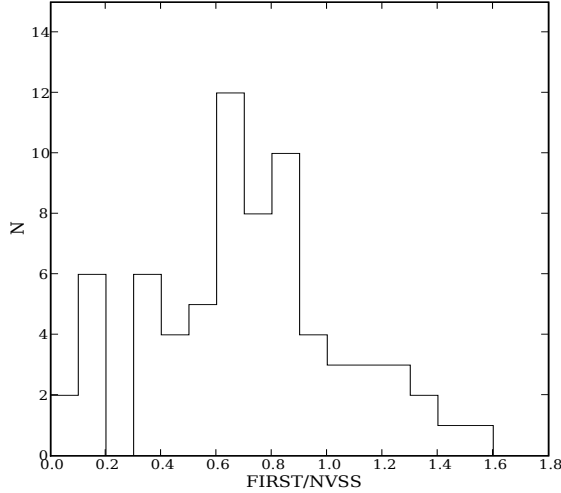


**Fig. 10.** Histogram of the flux ratio between the FIRST and NVSS detections for the CIGs.

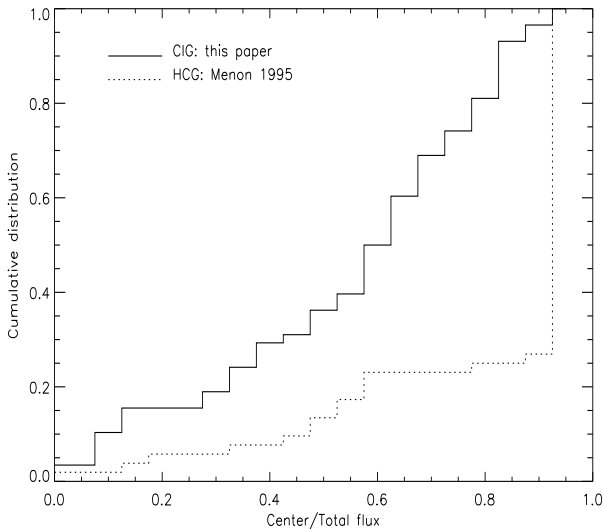


**Fig. 11.** Cumulative distribution of the FIRST/NVSS flux ratio for the CIG (solid line) and the center/total flux ratio (dotted line) from Menon (1995).

IRAS flux-limited sample ( $S_{60\mu\text{m}} > 2 \text{ Jy}$ ) were cross-matched with the NVSS (Yun et al. 2001), revealing that FIR-selected galaxies can account for the entire population of late-type field galaxies in the local Universe. Radio emission in these galaxies is mainly produced by star formation. One of the most recent radio continuum studies for a large sample involves the 2 degree Field Galaxy Survey (2dFGSDR2) cross-correlated with the NVSS for galaxies brighter than  $K = 12.75$  (Sadler et al. 2002). Using 2dF spectra, they found that 60% of the sources involve dominance of star formation and 40% AGN. Interpretation of all of these surveys is clouded by the uncertain role of environment. The AMIGA sample has the potential to clarify this role by providing a nurture-free local sample, large enough to permit evaluation as a function of source morphology and luminosity.

#### 4.1. 1.4 GHz radio luminosity function

The local RLF of the CIG sample is useful in order to get more insight into the cosmological evolution of the radio emission in isolated galaxies, as well as to compare them with other galaxy populations in the local Universe. We only compute the local RLF at 1.4 GHz, for which we can get an accurate statistics thanks to the large number of detections. To compute the RLF we follow the prescription given by Xu & Sulentic (1991). Since the CIG sample is optically selected, the RLF is derived from the OLF and the fractional bivariate function between the radio and optical luminosity. The OLF  $\phi(M)$  was estimated by Verdes-Montenegro et al. (2005) using the  $< V/V_m >$  test (Schmidt 1968) which indicates a high level of completeness for the CIG. The RLF is then calculated for that complete subsample.

The differential RLF  $\psi$  gives the number of galaxies per unit volume and per unit  $\log P_{1.4\text{GHz}}$  interval. It is derived as follows:

$$\psi(P) = 2.5\Delta M \sum_i \Theta(P|M_i)\phi(M_i) \quad (12)$$

where  $P = \log(P_{1.4\text{GHz}})$ .  $\Theta(P|M_i)$  is the bivariate (optical, radio) luminosity function (BLF). The factor 2.5 arises since  $\text{dex}(0.4) = 1$  magnitude. The BLF is defined as:

$$\Theta(P|M_i) = \frac{\mathcal{P}(P|M_i)}{\Delta P} \quad (13)$$

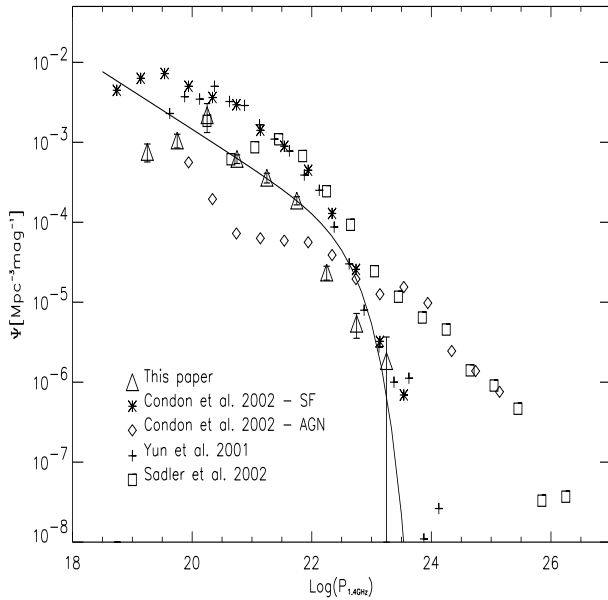
where  $\Delta P = 0.5$  and  $\mathcal{P}(P|M_i)$  is the conditional probability for a source with an absolute magnitude  $M$  ( $M_i + 0.5\Delta M \geq M > M_i - 0.5\Delta M$ ) to have the logarithm of its radio luminosity,  $\log(P_{1.4\text{GHz}})$ , within the interval  $[P - 0.5\Delta P, P + 0.5\Delta P]$ . In order to compute the BLF, we use the Kaplan-Meier estimator to take into account the upper limits of the radio observations, using the ASURV package. The errors of  $\psi(P)$  are the quadratic sums of the uncertainties of the OLF and the Kaplan-Meier estimator. The RLF is shown in Fig. 12 and the BLF is listed in Table 4. We point out that the inclusion of the upper limits in the computation may lead to a different final RLF compared with other studies, biased due to the use of only radio continuum detections. The survival analysis was designed to use the maximum of information available from the data and to provide a closer representation of the “true” distribution. The BLF is dominated by the small number statistics mainly at low optical and radio luminosity, due to the lack of faint galaxies in the CIG catalog. A clear correlation between the optical and radio luminosity shows up in the BLF, with the noticeable lack of galaxies with a strong radio continuum emission ( $\log(P_{1.4\text{GHz}}) \geq 23.50$ ). The RLF at 1.4 GHz is given in Table 5.

Figure 12 shows a comparison of the CIG RLF with other samples. Except for the AGN sample of Condon et al. (2002), all samples have a relatively similar RLF at low radio power ( $P_{1.4\text{GHz}} < 10^{22} \text{ W Hz}^{-1}$ ). The radio emission of these galaxies showing a similar contribution to the local density of the RLF is dominated by SF. At larger radio power, the 2dFGRS sample from Sadler et al. (2002) and AGN/UGC dominate the radio contribution, that is, the radio power is coming mainly from the AGN-powered galaxies. The CIG RLF decreases below the AGN dominated samples for powers higher than  $P_{1.4\text{GHz}} \sim 10^{23} \text{ W Hz}^{-1}$ , in very good coincidence with samples powered by SF. Thus, the radio emission from the CIG sample is mainly powered by SF and the AGN contribution is very low, as confirmed by Sabater et al. (2008).

The Schechter formalism to describe the luminosity function (Press & Schechter 1974) was initially developed to explain the

**Table 4.** Bivariate (optical,radio) luminosity function for the CIG sample.

$M$	-16.25	-16.75	-17.25	-17.75	-18.25	-18.75	-19.25	-19.75	-20.25	-20.75	-21.25	-21.75	-22.25
$\log(P)$													
18.75	0.00	0.00	0.00	0.00	0.00	0.00	0.00	0.00	0.00	0.00	0.00	0.00	0.00
19.25	0.00	0.00	0.00	0.81	0.31	0.83	0.00	0.00	0.00	0.00	0.00	0.00	0.00
19.75	0.00	0.00	0.00	0.81	0.94	0.28	0.63	0.40	0.00	0.00	0.00	0.00	0.00
20.25	2.00	0.00	0.00	0.37	0.42	0.26	0.16	0.13	0.35	0.00	0.00	0.00	0.00
20.75	0.00	0.00	0.00	0.00	0.25	0.46	0.70	0.65	0.77	0.47	0.45	0.31	0.00
21.25	0.00	0.00	0.00	0.00	0.08	0.17	0.39	0.57	0.47	0.61	0.34	0.00	1.07
21.75	0.00	0.00	0.00	0.00	0.00	0.00	0.12	0.24	0.35	0.73	0.83	1.22	0.00
22.25	0.00	0.00	0.00	0.00	0.00	0.00	0.00	0.00	0.04	0.14	0.29	0.38	0.93
22.75	0.00	0.00	0.00	0.00	0.00	0.00	0.00	0.00	0.00	0.04	0.10	0.09	0.00
23.25	0.00	0.00	0.00	0.00	0.00	0.00	0.00	0.00	0.01	0.00	0.00	0.00	0.00

**Fig. 12.** RLF at 1.4 GHz for the CIG sample (triangles) with 1- $\sigma$  error bars. The RLF is shown in  $\text{Mpc}^{-3} \text{mag}^{-1}$ . The line represents the Schechter fit to the CIG sample, taking into account only data points with  $\log(P) \geq 20.75$ .

luminosity function of galaxies based on the cosmological evolution of the clustering of matter in the Universe. Its application to radio frequencies (e.g. Yun et al. 2001; Serjeant et al. 2002) is a powerful tool to compare the distribution of various kinds of radio sources and to parametrize their evolution. The Schechter function for a RLF  $\rho(L)$  is the following:

$$\rho(L)dL = \rho_* \left(\frac{L}{L_*}\right)^\alpha \exp\left(-\frac{L}{L_*}\right) d\left(\frac{L}{L_*}\right) \quad (14)$$

where  $\rho_*$  and  $L_*$  are the characteristic density and luminosity of the population and  $\alpha$  describes the faint-end power-law slope for  $L \ll L_*$ . Our RLF cannot be well described by a single Schechter function. We therefore derived a fit only for the high luminosity data points, those with  $\log(P_{1.4\text{GHz}}) \geq 20.75$ . The fitted parameters are given in Table 6. The fits for Condon et al. (2002) and Yun et al. (2001) have been recomputed for consistency. The  $\chi^2$  of the fit is indicated together with the degree of freedom of the fit (DoF).

The  $L_*$  parameter is quite uncertain because of the relative larger errors of the bright end data. Yun et al. (2001) found that fitting

**Table 5.** RLF at 1.4 GHz for the CIG sample.

$\log P_{1.4\text{GHz}}$ ( $\text{W Hz}^{-1}$ )	$\psi$ ( $\text{Mpc}^{-3} \text{mag}^{-1}$ )	$N$
19.25	$1.9(\pm 0.5) \times 10^{-3}$	24.6
19.75	$2.6(\pm 5.5) \times 10^{-3}$	55.9
20.25	$5.5(\pm 2.1) \times 10^{-3}$	52.4
20.75	$1.6(\pm 0.2) \times 10^{-3}$	188.0
21.25	$9.0(\pm 0.1) \times 10^{-4}$	144.6
21.75	$4.7(\pm 0.5) \times 10^{-4}$	165.7
22.25	$5.9(\pm 0.1) \times 10^{-5}$	39.8
22.75	$1.3(\pm 0.5) \times 10^{-5}$	10.0
23.25	$4.6(\pm 4.6) \times 10^{-6}$	1.0

**Table 6.** Schechter function for the RLF at 1.4 GHz.

Survey	$\rho_*$ ( $\times 10^{-3}$ )	$L_*$ ( $\times 10^{23}$ )	$\alpha$	$\chi^2/\text{DoF}$
CIG	$34.2(\pm 9.0)$	$0.43(\pm 0.23)$	$-0.47(\pm 0.06)$	0.04/3
UGC-SF <sup>1</sup>	$46.8(\pm 31.0)$	$0.94(\pm 0.24)$	$-0.48(\pm 0.08)$	0.1/10
IRAS-2Jy <sup>2</sup>	$19.6(\pm 13.8)$	$2.30(\pm 1.30)$	$-0.73(\pm 0.11)$	0.8/14

<sup>1</sup> Condon et al. (2002), SF sample.<sup>2</sup> Yun et al. (2001).

their RLF with a sum of two Schechter functions gives a better fit. We tried such decomposition for the CIG sample, and the  $\chi^2$  was not improved but increased. It shows the limit of the application of the Schechter formalism to the RLF, developed to model the mass distribution of the sub-structures in the formation of the galaxies. Yun et al. (2001) noted that their decomposition fits two different galaxy populations: one normal, late-type field galaxies, and a second composed of starburst and luminous infrared galaxies. It appears that the “field” galaxies of the IRAS-2 Jy sample have a closer Schechter decomposition to the CIG population than the starburst galaxies with  $L_* \sim 2 \times 10^{22} \text{ W Hz}^{-1}$  and  $\alpha \sim -0.63$ . The lower power-law slope of the CIG compared to the UGC-SF sample indicates that the CIG sample has a larger population of low luminosity galaxies. The same conclusion arises from the lower  $L_*$  value than the IRAS-2 Jy, since they have a comparable power-law slope.

#### 4.2. Radio power density

We chose to compute the total radio power density from the RLF at 1.4 GHz rather than from the Schechter fit, since the parameters of the Schechter fit would give the total power density as  $U_{1.4\text{GHz}} = \rho_* L_* \Gamma(2 + \alpha)$  for a larger range than the

**Table 7.** Radio power density.

Survey	$U_{1.4\text{GHz}}$ $10^{18} \text{ W Hz}^{-1} \text{ Mpc}^{-3}$	References
CIG	$4.44 \pm 0.52$	This paper
IRAS-2Jy	$15.60 \pm 0.25$	Yun et al. (2001)
UGC/NVSS-SF	$17.06 \pm 0.35$	Condon et al. (2002)
UGC/NVSS-AGN	$41.88 \pm 3.47$	Condon et al. (2002)
2dFGRS	$74.76 \pm 3.59$	Sadler et al. (2002)

available radio data. Given the uncertainties on the parameters and the extrapolation of the formula, we preferred to compute  $U_{1.4\text{GHz}}$  only on the radio power range of the RLF. The results for the CIG and the other samples considered from the bibliography are given in Table 7: the radio power density for each sample is computed for a Hubble constant of  $H_0 = 75 \text{ km s}^{-1}$ . The CIG sample has, by far, the lowest contribution ( $4.4 \times 10^{18} \text{ W Hz}^{-1} \text{ Mpc}^{-3}$ ) in the Local Universe to the radio continuum emission at 1.4 GHz. Its contribution is 30% of the total power density of the IRAS-2 Jy sample and 6% compared to the 2dFGRS, which covers a redshift range of  $z = 0.005$  to  $0.438$  and has 60% of active galaxies and 40% of star-forming galaxies (Sadler et al. 2002). The difference of the total radio luminosity between the UGC and IRAS-2 Jy samples is mainly due to the lower faint end of the later one. It appears clearly that the galaxies hosting an AGN are dominating the sources emitting at 1.4 GHz. The low contribution of the CIG galaxies to the total radio power density is the combination of two effects: (i) a slightly lower radio emission of the individual galaxies, in comparison to other environments, as shown for the mean  $\log(L)$  in comparison to the UGC-SF sample of Condon et al. (2002), and (ii) a low number density of isolated galaxies in the local Universe.

## 5. Conclusions

This paper is part of a series designed to characterize the ISM in a sample of the most isolated galaxies in the local Universe. We are establishing multiwavelength baselines or zero-point levels for the stellar content and the different components of the ISM against which samples in different environments can be compared and interpreted. Radio continuum emission that arises from either star formation or active nuclei should be at the lowest “natural” level in the AMIGA sample. We analyzed radio continuum emission at three frequencies: 325 MHz, 1.4 and 4.8 GHz using data from the WENSS, NVSS, FIRST and GB6 surveys.

1. We compare the CIG radiocontinuum power at 1.4 GHz with the one of the UGC-SF sample (Condon et al. 2002) of field star-forming galaxies. The sample is similar in distance and optically brighter. Taking into account the upper-limits by using the survival analysis, the mean of  $\log(P)$  for the CIG sample (20.11) appears significantly lower than for the UGC-SF sample (21.61).
2. Radio-to-optical flux ratios ( $R$ ) show a median value  $\sim 4.5$ , confirming that radio emission in our sample is largely due to star formation. Comparison with a sample of emission line galaxies (van Dуйne et al. 2004) reveals striking differences, with most  $R$  values between 10–100, while most of our sample lies in an order of magnitude lower range, between  $R = 1$ –10, similar to the one of the UGC-SF sample.
3. The 1.4 GHz detection fraction for FIRST is much lower than for NVSS even though FIRST is a more sensitive sur-

vey. This is because the spatial frequency attenuation in FIRST makes it sensitive only to compact, largely nuclear, emission in our sample galaxies. An isolated sample like AMIGA should be dominated by disk star formation which FIRST cannot see. Thus NVSS, which is sensitive to this emission, detects far more galaxies, and we estimate that disk emission dominates the radio continuum signature of  $\sim 80\%$  of our largely spiral sample. Nuclear emission is thought to be enhanced by interactions that dissipate angular momentum leading to gas infall. Dissipative effects are likely near minimum in our sample. This can be contrasted to surveys of compact groups (Menon 1995) where most radio detections involve compact nuclear emission and where quasi-continuous tidal perturbations should efficiently channel any unstripped gas into the centers of the galaxies.

4. Isolated early-type (E/S0) galaxies are one of the most intriguing, albeit small ( $\sim 14\%$ ), parts of the AMIGA sample. They show a similar detection fraction to that of the spirals which already marks them as unusual. If they are true early-types then it is difficult to ascribe their radio emission to star formation. Either many of them are misclassified spirals, or isolated early-types are somehow slightly hyperactive (unusual star formation?, sites of minor mergers?). The number of radio detection of S0 galaxies is similar to the ellipticals and show comparable radio luminosities. Since S0 show less association with active nuclei these detections may be telling us that: 1) some S0 could be misclassified ellipticals and 2) others could be misclassified spirals.
5. The RLF for our sample was derived using the radio-optical bivariate function. It also suggests that radio emission in our isolated sample is star formation dominated. It shows a strong drop at  $P_{1.4\text{GHz}} \sim 10^{23} \text{ W Hz}^{-1}$ , with little contribution from nuclear activity (see also Sabater et al. 2008).
6. The RLF allowed us to compute the total radio power density at 1.4 GHz for our sample. We found:  $U_{1.4\text{GHz}} \sim 4.4 \times 10^{18} \text{ W Hz}^{-1} \text{ Mpc}^{-3}$ , compared to  $15.6 \times 10^{18}$  for the IRAS-2 Jy sample,  $17.1 \times 10^{18}$  for the UGC-SF sample,  $41.9 \times 10^{18}$  for the UGC-AGN sample, and  $74.8 \times 10^{18}$  for the 2dFGRS sample. AMIGA gives at most 30% of the contribution of other star-forming samples and 10% of AGN-dominated samples.

AMIGA provides a unique reference sample for studies that aim to quantify the effects of environment. This is true whether one studies interacting samples (e.g. pairs, compact groups) dominated by one-on-one encounters or simply galaxies in environments with different average surface densities.

**Acknowledgements.** We thank the anonymous referee for a careful reading and very detailed report which helped to improve this paper significantly. SL, LVM, JSM, DE, UL, SV, GB and EG are partially supported by DGI Grant AYA 2005-07516-C02 and Junta de Andalucía (Spain). SL was partially supported by an Averroes Fellowship contract from the Junta de Andalucía. UL is supported by a Ramon y Cajal fellowship contract and acknowledges support from the DGI grant ESP2003-00915. GB is supported at the IAA/CSIC by an I3P contract (I3P-PC2005-F) funded by the European Social Fund. This research has made use of the NASA/IPAC Extragalactic Database (NED) which is operated by the Jet Propulsion Laboratory, California Institute of Technology, under contract with the National Aeronautics and Space Administration.

## References

- Allen, R. J., Ekers, R. D., Burke, B. F., & Miley, G. K. 1973, *Nature*, 241, 260
- Becker, R. H., White, R. L., & Helfand, D. J. 1995, *ApJ*, 450, 559
- Benn, C. R., Rowan-Robinson, M., McMahon, R. G., Broadhurst, T. J., & Lawrence, A. 1993, *MNRAS*, 263, 98
- Bertin, E., & Arnouts, S. 1996, *A&AS*, 117, 393
- Condon, J. J. 1980, *ApJ*, 242, 894

- Condon, J. J., Condon, M. A., Gisler, G., & Puschell, J. J. 1982, *ApJ*, 252, 102
- Condon, J. J. 1984, *ApJ*, 284, 44
- Condon, J. J. 1989, *ApJ*, 338, 13
- Condon, J. J., Cotton, W. D., Greisen, E. W., et al. 1998, *AJ*, 115, 1693
- Condon, J. J., Cotton, W. D., & Broderick, J. J. 2002, *AJ*, 124, 675
- Domingue, D. L., Sulentic, J. W., & Durbala, A. 2005, *AJ*, 129, 2579
- Feigelson, E. D., & Nelson, P. I. 1985, *ApJ*, 293, 192
- Gregory, P. C., Scott, W. K., Douglas, K., & Condon, J. J. 1996, *ApJS*, 103, 427
- Hummel, E. 1980, *A&A*, 89, L1
- Hummel, E. 1981, *A&A*, 93, 93
- Karachentseva, V. E. 1973, *SoSAO*, 8, 3
- Kennicutt, R. C. Jr., Roettiger, K. A., Keel, W. C., van der Hulst, J. M., & Hummel, E. 1987, *AJ*, 93, 1011
- Lavalley, M., Isobe, T., & Feigelson, E. 1992, *ADASS I*, ASP Conf. Series, Vol. 25, D. M. Worrall, C. Biemesderfer, and J. Barnes, eds., p. 245.
- Leon, S., & Verdes-Montenegro, L. 2003, *A&A*, 411, 391
- Lisenfeld, U., Verdes-Montenegro, L., Sulentic, J., et al. 2007, *A&A*, 462, 507
- Menon, T. K. 1992, *MNRAS*, 255, 41
- Menon, T. K. 1995, *MNRAS*, 274, 845
- Menon, T. K. 1999, *Ap&SS*, 269, 435
- Press, W. H., & Schechter, P. 1974, *ApJ*, 187, 425
- Rengelink, R. B., Tang, Y., de Bruyn, A. G., et al. 1997, *A&AS*, 124, 259
- Sabater, J., Leon, S., Verdes-Montenegro, L. et al. 2008, *A&A* in press
- Sadler, E. M., Jackson, C. A., Cannon, R. D., et al. 2002, *MNRAS*, 329, 227
- Serjeant, S., Gruppioni, C., & Oliver, S. 2002, *MNRAS*, 330, 621
- Schmidt, M. 1968, *ApJ*, 151, 393
- Stocke, J. T., Tifft, W. G., & Kaftan-Kassim, M. A. 1978, *AJ*, 83, 322
- Stocke, J. T. 1978, *AJ*, 83, 348
- Sulentic, J. W. 1976a, *AJ*, 81, 582
- Sulentic, J. W. 1976b, *ApJS*, 32, 171
- Sulentic, J. W., Zamfir, S., Marziani, P., et al. 2003, *ApJ*, 597, L17
- Sulentic, J. W., Verdes-Montenegro, L., Bergond, G., et al. 2006, *A&A*, 449, 937
- Tovmassian, H. M. 1968, *Australian Journal of Physics*, 21, 193
- Van Duyne, J., Beckerman, E., Salzer, J. J., et al. 2004, *AJ*, 127, 1959
- Verdes-Montenegro, L., Sulentic, J., Lisenfeld, U., et al. 2005, *A&A*, 436, 443
- Verley, S., Odewahn, S. C., Verdes-Montenegro, L., et al. 2007a, *A&A*, 470, 505
- Verley, S., Leon, S., Verdes-Montenegro, L., et al. 2007b, *A&A*, 472, 121
- Wright, A. E. 1974, *MNRAS*, 167, 251
- Xu, C., & Sulentic, J. W. 1991, *ApJ*, 374, 407
- Young, J. S., & Knezek, P. M. 1989, *ApJ*, 347, L55
- Yun, M. S., Reddy, N. A., & Condon, J. J. 2001, *ApJ*, 554, 803